Atmos. Meas. Tech. Discuss., doi:10.5194/amt-2016-185, 2016
Manuscript under review for journal Atmos. Meas. Tech.
Published: 12 July 2016

Atmospheric Measurement Techniques Discussions

Improved MODIS Dark Target Aerosol Optical Depth algorithm over land: Angular effect Correction

Yerong Wu[1], Martin de Graaf[1,2], and Massimo Menenti[1]

[1]Department of Geoscience and Remote Sensing (GRS), Delft University of Technology (TUDelft), Stevinweg 1, 2628 CN Delft, The Netherlands.
[2]Royal Netherlands Meteorological Institute (KNMI), Wilhelminalaan 10, De Bilt 3732 GK, The Netherlands.

Correspondence to: Yerong Wu (yerong.wu@tudelft.nl)

Abstract. Aerosol Optical Depth (AOD) retrieved from MOderate Resolution Imaging Spectroradiometer (MODIS) measurements over land, can be improved by taking into account the surface Bidirectional Reflectance Distribution Function (BRDF), as shown in a previous study (Wu et al., 2016). However, the relationship of the surface reflectance between visible and short wave Infrared band that applied in the previous study, can lead to an angular dependence of the AOD retrieval. This has at least two reasons. The relationship based on the assumption of isotropic reflection or Lambertian surface is not suitable for the surface directional-directional reflectance. On the other hand, although the relationship varies with the surface cover type by considering the vegetation index $NDVI_{SWIR}$, this index itself has a directional effect and affects the estimation of the surface reflection, and finally can lead to some errors in the AOD retrieval. To improve this situation, we derived a new relationship for the spectral surface directional-directional reflectance in this study, using 3 years of dataset from AERONET-based Surface Reflectance Validation Network (ASRVN). To test the performance of the new algorithm, three case studies were used: 2 years of data from Eastern China and North America, and 4 months of data from the global land. The results show that the angular effects of the AOD retrieval are largely reduced in most cases. Particularly, for the global land case, the AOD retrieval was improved by the new algorithm compared to the previous study and MODIS collection 6 dark target algorithm, with the increase of 2.5% and 5% AOD retrievals falling within the expected accuracy level $\pm$(0.05+15%), respectively.

1 Introduction

The atmospheric aerosol is a suspension of liquid and solid particles distributed in the air with a radius ranging from a few nm to larger than 100 nm. Aerosols from natural sources (e.g., volcanic ash, sea spray aerosol, and dust) and human activities (e.g., industrial emission, forest fire smoke and fossil fuel burning aerosol) play a key role in climate and environment, and human health. Near land surfaces, high concentrations of fine aerosols with various micro-organisms can be inhaled by humans and cause human diseases (Laden et al., 2000; Samet et al., 2000; Pope III et al., 2002; Pope III and Dockery, 2006). On the other hand, aerosols have a significant impact on climate due to their direct and indirect effects (Kaufman et al., 2002; IPCC, 2013). Most of the aerosols affect the climate by cooling the atmosphere through reflecting solar radiation into outer space, whereas absorbing aerosols (e.g., black carbon) warm the atmosphere, this is also called the direct effect of aerosol. The net effect of

Atmos. Meas. Tech. Discuss., doi:10.5194/amt-2016-185, 2016
Manuscript under review for journal Atmos. Meas. Tech.
Published: 12 July 2016

Atmospheric Measurement Techniques Discussions

aerosols is cooling. As for indirect effects on climate, aerosols can play a role as cloud condensation nuclei and influence the formation and albedo of the cloud.

Aerosols present a strong variability in space and time due to their short lifetime (from a few hours to a week). Therefore, monitoring aerosols on a daily basis is necessary. To describe the magnitude of the absorption and scattering of incident light by aerosol particles, and also to some degree indicate surface aerosol amount (Chu et al., 2003; Engel-Cox et al., 2004; Wu et al., 2012), Aerosol Optical Depth (AOD) has gained more attention. Many AOD products have been produced by inversing the radiative transfer model using satellite measurements (Martonchik et al., 1998; Diner et al., 2005; North et al., 1999; North, 2002; Dubovik et al., 2011; Hsu et al., 2004; Remer et al., 2005; Levy et al., 2007b, a). The MODIS AOD product, due to the maturity of its algorithm and nearly daily coverage over the globe, has been extensively used in scientific research. Currently, the MODIS Collection 6 Dark Target (C6_DT) AOD product over ocean has a relatively high accuracy with +(0.04 + 10%), -(0.02 + 10%), and a relatively low accuracy over land with $\pm$(0.05 + 15%) (Levy et al., 2013). The accuracy of the retrievals over land should be improved for global climate research (e.g. McComiskey et al., 2008).

The AOD retrieval is a more challenging task over land than over ocean since the land surface is much brighter than the ocean surface. Specifically, the contribution from the bright surface to the TOA radiance can be higher than the one from the atmosphere, which makes it difficult to separate the aerosol and surface contributions to the TOA radiance. For this reason, two versions of the MODIS Dark Target and Deep Blue AOD algorithm were developed over the dark (e.g., vegetated area) (Remer et al., 2005, 2013; Levy et al., 2007a, b, 2013) and bright surface (e.g, desert and urban area) (Hsu et al., 2004, 2006), respectively. These two algorithms take advantage of dark or darker surfaces at different bands to obtain a relatively accurate estimation of the atmosphere contribution to the radiance at TOA, although they aim at different surface types. MODIS DT land AOD algorithm makes use of the presence of a dark surface in two visible channels 0.47- and 0.66 μm and the approximate transparency of the atmosphere at a relatively long wavelength 2.12 μm, to combine the effect of the atmosphere scattering and surface reflection on the TOA radiance. MODIS Deep Blue AOD algorithm addresses the issue on the surface brightness in a similar way, but utilizing the characteristics of the darker surface in two blue channels 0.412- and 0.470 μm and little absorption by dust in a red channel (e.g., 0.670 μm).

However, using the presence of the dark surface in a few channels, it leads to the limited MODIS observations (two or three single-view channels) in the retrieval. The limited observations do not allow us to directly solve the Radiative Transfer (RT) process or equation since there are more unknowns than observations. The spectral surface reflectance needs to be constrained to solve the RT process, leading the AOD retrieval. Thus, some methods are developed for the AOD retrieval over land, by using ancillary data and "a priori" assumptions to constrain or determine the surface reflectance.

To obtain the surface reflectance from the satellite-observed radiation field, one needs to subtract the atmospheric effects (called the atmospheric correction) by assuming/knowing aerosol parameters and atmospheric components. Using the minimum reflectivity technique (Herman and Celarier, 1997; Koelemeijer et al., 2003), a database for the global surface reflectance is generated, and applied to the first generation of Deep Blue algorithm (Hsu et al., 2004, 2006). By combining surface reflectance database and dynamic surface reflectance determination, a hybrid method has been used for the retrieval over a general surface (Hsu et al., 2013). As for C5 and C6 DT over land, the relationship was derived for the surface reflectance

Atmos. Meas. Tech. Discuss., doi:10.5194/amt-2016-185, 2016
Manuscript under review for journal Atmos. Meas. Tech.
Published: 12 July 2016

Atmospheric Measurement Techniques Discussions

at visible wavelengths 0.466- and 0.644 μm versus short wave Infrared 2.12 μm (VISvsSWIR), by considering vegetation amount and the scattering angle (Levy et al., 2007b, 2013).

Following the dark surface selection in C6_DT algorithm but considering the anisotropic reflection of the surface, a new AOD retrieval algorithm called BRF_DT was developed (Wu et al., 2016). Although the BRF_DT AOD was improved compared to C6_DT one, the surface reflectance parameterization inherited from C6_DT algorithm needs to be further refined to achieve better retrievals. The derived relationship based on the assumption of isotropic reflection surface (Lambertian surface) is not quite suitable for the BRF_DT algorithm which requires a relationship for the spectral surface Bidirectional Reflectance Factor (BRF, or directional-directional reflectance). Although the relationship in C6_DT takes into account the angular effect (e.g, regarding the scattering angle as a variable), this effect brought by the index of vegetation amount or "greenness" — Normalized Distribution Vegetation Index ($NDVI_{SWIR}$) in the relationship, is not well evaluated and investigated. As a result, directly applying the parameterization leads to the dependence of AOD retrieval on the observation and illumination geometry in BRF_DT algorithm, giving a underestimation and overestimation of the AOD at a small and large scattering angle, respectively.

This study aims at improving the BRF_DT algorithm by updating the parameterization of the spectral surface BRF. The improved BRF_DT algorithm is called BRF_DT2 here. The paper is organized into several sections. Section 2 introduces the derivation of the relationship of the spectral surface BRF for VISvsSWIR using 3 years (2005-2007) of data which is from AERONET-based Surface Reflectance Validation Network (ASRVN) dataset. Section 3 presents the AOD retrieval by the new algorithm, and its validation with AERONET measurements. The AOD retrievals of the current and operational MODIS C6_DT algorithm and the previous BRF_DT algorithm are also put here to make a cross-comparison and get a better understanding of the difference among the algorithms. Conclusions are made in section 4.

2 The development of BRF Dark Target 2 algorithm

The accurate calculation of the TOA radiance requires considering the anisotropic reflection of the surface. Thus, we built a frame work of RT process by coupling the non-Lambertian surface.

Following the four-stream theory (Verhoef, 1985), the radiation field in our study is divided into directional (d), and hemispheric part (h) indexed as the subscript symbol "d" and "h". Since we have an incident and reflected radiation, thus we get four combinations of these two symbols: "dd", "dh", "hd" and "hh". The symbol "i" and "v" indicate the direction of an incident or solar (solar zenith angle θ_s, and solar azimuth angle ϕ_s) radiation and the direction of reflected radiation into the view of the sensor (sensor zenith angle θ_v and sensor azimuth angle ϕ_v), respectively (see Figure 1).

A sketch diagram is shown for the TOA radiance observed by the satellite considering the surface BRDF effects in Figure 2. In this figure, we have a solar beam F_0 with a zenith angle θ_s as the incident radiation into the atmosphere. The incident radiation is then scattered or reflected back into space and forward transmitted in the atmosphere. The radiance reflected by the atmosphere into the view of the sensor is called "path reflected radiance" ρ^a. The forward transmitted radiation reaches the lower atmosphere, being partly scattered and partly attenuated by the atmosphere. The scattered and attenuated parts, called diffuse and directional flux $t_{dd}(i)$ and $t_{dh}(i)$, respectively, give the downward transmitted radiance. Since the underlying surface is

Atmos. Meas. Tech. Discuss., doi:10.5194/amt-2016-185, 2016
Manuscript under review for journal Atmos. Meas. Tech.
Published: 12 July 2016

Atmospheric Measurement Techniques Discussions

non-lambertian, the anisotropic reflection of the surface is simply described as 4 elements: hemispherical-directional ① (R_{hd}), hemispherical-hemispherical ② (R_{hh}), directional-directional ③ (R_{dd}) and directional-hemispherical reflection/reflectance ④ (R_{dh}), respectively, see Figure 2. The downward transmitted radiance undergoes complicated reflections between the surface and the atmosphere.

The directional flux reflected by the surface could be from the downward transmitted radiance after ①③, whereas the corresponding hemispherical one is from the downward transmitted radiance by ②④. Here we neglect the multiple reflections between the lower atmosphere and the surface (e.g., strong mirror reflection) for the directional flux, but for the hemispherical-hemispherical flux where the atmosphere backscattering ratio is denoted as s. Finally, there is a directional flux from the lower atmosphere, through the directional transmission $t_{dd}(v)$ into the view of the sensor. Similarly, the sensor receives another directional flux which is from the diffuse flux undergoing the hemispherical-directional transmission $t_{hd}(v)$.

Therefore, the TOA reflectance received by the sensor (radiance converted to reflectance by normalization) is composed of two parts: the atmospheric reflectance or path reflectance, the reflectance contributed by the interaction of the surface and the atmosphere, which is written as follows (a complete deduction has been given by (Wu et al., 2016)):

$$\rho^*(i,v) \quad = \quad \rho^a(i,v) + \frac{\mathbf{T}(i)\mathbf{R}(i,v)\mathbf{T}(v) - t_{dd}(i)\,|\mathbf{R}(i,v)|\,t_{dd}(v)s}{1 - R_{hh}s}, \tag{1}$$

where,

$$\begin{aligned} \mathbf{R}(i,v) &= \begin{bmatrix} R_{dd} & R_{dh} \\ R_{hd} & R_{hh} \end{bmatrix} \\ \mathbf{T}(i) &= \begin{bmatrix} t_{dd}(i) & t_{dh}(i) \end{bmatrix} \\ \mathbf{T}(v) &= \begin{bmatrix} t_{dd}(v) \\ t_{hd}(v) \end{bmatrix} \end{aligned} \tag{2}$$

For convenience, the dependence of each term on wavelength λ is not explicitly shown here and in subsequent equations. The second term on the right side of equation 1 shows the contribution of the surface to TOA reflectance. $\mathbf{R}$ is the surface reflecting-matrix, which is made up of four components R_{dd}, R_{dh}, R_{hd} and R_{hh}. Its determinant form is $|\mathbf{R}| = R_{dd}R_{hh} - R_{dh}R_{hd}$.

Compared to the C6_DT algorithm, three more unknowns (R_{dh}, R_{hd} and R_{hh}) are in our study, which require to be solved by the ancillary data. We make use of surface BRDF/albedo product 8-day MCD43A1 (500 m resolution) for the determination of the three unknowns in the surface reflectance matrix (Lucht et al., 2000; Schaaf et al., 2002). MCD43A1 product utilizes three scattering kernels of Lambertian, geometric-optical and volume (also called RossThick-LiSparse (LSRT) model) to reconstruct the surface reflectance R_{dh} and R_{hh} by a linear combination. R_{hd} is obtained from R_{dh} by assuming that reciprocity law is valid for the surface reflectance when $v = i$. The directional-directional reflectance R_{dd} (or BRF) is numerically equivalent to the BRDF multiplied by π. The surface BRF R_{dd} will be retrieved in the algorithm as other two parameters (AOD and fine ratio). The parameterization of the spectral surface BRF for VISvsSWIR in Wu et al. (2016) is reconsidered and updated here, described below.

Atmos. Meas. Tech. Discuss., doi:10.5194/amt-2016-185, 2016
Manuscript under review for journal Atmos. Meas. Tech.
Published: 12 July 2016

Atmospheric Measurement Techniques Discussions

2.1 The VISvsSWIR surface BRF

The BRF data from ASRVN dataset "IBRF" is used to derive the BRF relationship for VISvsSWIR for the new algorithm. In the ASRVN algorithm (Wang et al., 2009), the LSRT model is integrated into Radiative Transfer (LSRT-RT) to generate accurate TOA reflectance. Using the information in aerosol and water vapor from AERONET (about 100 sites), three LSRT BRDF model parameters and the surface BRF are retrieved in the ASRVN algorithm by fitting the simulated TOA reflectance to the observed one over 4- to 16-day period .

Three years (2005-2007) of ASRVN data from Terra satellite was collected, where the dataset is given as a box of 50 $\times$ 50 pixels (1-km resolution) collocated with AERONET sites. More than 28,000 cases were collected. Only cases with more than 80% good quality (ASRVN Quality Assurance = 0) and low aerosol loading (AOD < 0.2) over 10 $\times$ 10 km^2 area were chosen for analysis (5518). Under low aerosol loading, the radiation observed by the satellite is expected to be dominated by the directional component reflected by the surface since the directional incident radiation is less scattered by the atmosphere. In this case, the BRF retrieval is expected to be more accurate than that under heavy aerosol loading. Actually, considering all condition of AOD (9014 cases), the relationship for the spectral surface BRF gives a difference by 6% compared to that with low aerosol loading. Figure 3 shows the scatter plot of the surface BRF at visible (0.466- and 0.644 μm) and 2.12 μm (AOD < 0.2). High correlation coefficients (R: 0.872 and 0.967) of 0.466- to 2.12 μm (0.466vs2.12) and 0.644- to 2.12 μm (0.644vs2.12) are found, respectively.

To check whether the relationships in Figure 3 are dependent on the surface brightness, we perform similar regressions on the dataset (2739 cases) where the dark surface is selected which are defined by $R_{dd,0.466} < 0.06$, $R_{dd,0.644} < 0.15$ and $R_{dd,2.12} < 0.25$. For 0.466vs2.12 and 0.644vs2.12, the correlation coefficients become low, with the R reduced from 0.872 and 0.967 to 0.559 and 0.929, respectively. And the slopes are reduced from 0.42 and 0.82 to 0.20 and 0.55. The changes of the regression demonstrate that the surface brightness has a strong impact on the spectral surface BRF relationship. As we know, the DT AOD algorithm requires that the surface brightness are expected to be dark after masking the pixels of cloudy, water and snow/ice, where the dark targets are selected over the 20 $\times$ 20 pixels box (500 m resolution) with the measured 2.12 μm reflectance ranging from 0.01 and 0.25, by removing brightest 50% and darkest 20% of the measured 0.66 μm reflectance (Remer et al., 2005; Levy et al., 2007b, 2013). Therefore, the relationship needs to be investigated over the dark surface to improve the AOD retrieval. The dataset (2739 cases) filtered by $R_{dd,0.466} < 0.06$, $R_{dd,0.644} < 0.15$ and $R_{dd,2.12} < 0.25$ is used for further investigation. Meanwhile, we note that over the dark surface the low correlation coefficients was found for VISvsSWIR especially for 0.466vs2.12, which implies that the relationship may be dependent on other factors such as surface type and observation and illumination geometry.

2.2 Variability of the VISvsSWIR surface BRF: scattering angle

Many studies did show that the spectral surface relationship over a dark surface is dependent on the observation and illumination geometry (Remer et al., 2001; Gatebe et al., 2001; Levy et al., 2007b). Although these studies were done with the lambertian surface, the dependence of the spectral BRF is expected to be similar to that with the lambertian surface since the difference of

Atmos. Meas. Tech. Discuss., doi:10.5194/amt-2016-185, 2016
Manuscript under review for journal Atmos. Meas. Tech.
Published: 12 July 2016

Atmospheric Measurement Techniques Discussions

the TOA reflectance between a non-Lambertain and Lambertian surface is expected to be small under the clear sky (e.g., AOD < 0.2) (Wu et al., 2016).

The dependence is mainly caused by the biological feature of vegetations or plant canopies. Plant canopies are not randomly oriented (Rondeaux and Vanderbilt, 1993), which could lead to the difference of the surface BRF ratio for VISvsSWIR on the different angles. On the other hand, the dependence could be largely reduced over the dry/dead vegetation or black soil area, since the surface BRF ratio for this area is expected to be the same for different angles. Thus, we evaluate the dependence of the surface BRF ratio for VISvsSWIR on the angle.

Generally, the illumination and view angle is characterized: solar zenith angle, solar azimuth angle, sensor zenith angle and sensor azimuth angle. To simplify illumination and view angle, we use one variable — the scattering angle instead. The scattering angle Θ is a function of these four angles, defined as follows (see Figure 1):

$$\Theta = cos^{-1}(-cos\theta_s cos\theta_v + sin\theta_s sin\theta_v cos(\phi_s - \phi_v)) \quad (3)$$

Sorted by the scattering angle, the dataset (2739 cases) was put into 20 groups of equal size (about 140 points for each bin of the scattering angle). Figure 4 presents the relationships of the surface BRF VISvsSWIR as a function of the scattering angle. The median values of each bin of the scattering angle were used for the linear regression. The slope and offset are similar to that in Figure 3, but replaced with one parameter — the ratio between the surface BRF of VISvsSWIR in Figure 4.

Figure 4 d and e present the ratios of the surface BRF for 0.466/2.12 and 0.644/2.12, respectively. The slope for 0.644/2.12 ratio (0.00027) is much smaller (nearly 9 times) than that for 0.466/2.12 ratio (0.00227). This is mainly due to the different absorption at different wavelengths and scattering angles over the vegetation area. At 0.466 μm, the vegetation area performs more absorption at a small scattering angle (e.g., $\Theta < 110°$), while less at a large scattering angle (e.g., $\Theta > 150°$) (see Figure 4 a). It is not the case at the other two wavelengths (0.644- and 2.12 μm) , where the vegetation area performs a similar absorption at these two wavelength, showing a light increase of absorption as increasing the scattering angle (see Figure 4 b and c). As result, the ratio for 0.644/2.12 is much less dependent on the scattering angle than that for 0.466/2.12.

2.3 Directional effect of $NDVI_{SWIR}$ in the VISvsSWIR surface BRF

As we discussed above, the relationship of VISvsSWIR surface BRF is dependent on the surface brightness or surface type. This requires us to take the surface type into account in the relationship. Although $NDVI_{SWIR}$ has been extensively used to constrain the spectral surface reflectance in the AOD retrieval (Levy et al., 2013; Hsu et al., 2013), the directional effect of the index needs to be reconsidered. To test the directional effect of $NDVI_{SWIR}$, the measured reflectance at 1.24 μm $\rho^m_{1.24}$ and 2.12 μm $\rho^m_{2.12}$ in $NDVI_{SWIR}$ that match the ASRVN dataset were collected. The observations are also filtered by the dark surface (defined in section 2.1), and shown in Figure 5 as a function of the scattering angle ($\rho^m_{1.24}$vsSCA and $\rho^m_{2.12}$vsSCA).

The measurements present different dependence on the scattering angle, where a higher correlation coefficient R was found for the reflectance $\rho^m_{1.24}$ than for the reflectance $\rho^m_{2.12}$, with the absolute value of 0.89 and 0.47, respectively. As for $NDVI_{SWIR}$ (not shown here), it does not show much dependence on the scattering angle due to its nonlinear transformation that neutralizes the dependence of the two measurements, but it does change due to their dependence. For example, we take

Atmos. Meas. Tech. Discuss., doi:10.5194/amt-2016-185, 2016
Manuscript under review for journal Atmos. Meas. Tech.
Published: 12 July 2016

Atmospheric Measurement Techniques Discussions

the median values of the 1.24- and 2.12 μm measurements at the scattering angles of 110°, 160° for the discussion. Based on the regression equation in Figure 5, the calculated $NDVI_{SWIR}$ at these two angles yields a significant difference (37%), with the value of 0.358 and 0.493 for 110° and 160°, respectively. The directional effects of $NDVI_{SWIR}$ is caused by the absorption of green vegetation on the different angles. These effects can further significantly affect the AOD retrieval in MODIS DT algorithm, since $NDVI_{SWIR}$ is viewed as one of the free variables in the parameterization of MODIS dark surface reflectance.

However, it is not easy to correct the directional effects of the MODIS observation. If we simply follow the linear regression relationship in Figure 5, the directional effects for 1.24- and 2.12 μm observations and the corresponding $NDVI_{SWIR}$ will be poorly corrected since there is still a large uncertainty in the relationship. On the other hand, by removing $NDVI_{SWIR}$ from the relationship of VISvsSWIR surface BRF, the AOD retrieval does not differ too much from the one keeping $NDVI_{SWIR}$ in the relationship, with the difference of $< 1\%$ for the global land area.

2.4 Final parameterization of the VISvsSWIR surface BRF

Results of three years ASRVN BRF dataset over around 100 AERONET sites show that the ratio of surface VISvsSWIR BRF has a strong dependence on the scattering angle and surface type. Due to the disturbance of the directionality by 1.24- and 2.12 μm observations, the "greenness" index $NDVI_{SWIR}$ will not be taken into account in the relationship of the spectral surface BRF. Particularly, considering the overestimation of the regressed relationship for surface BRF 0.466/2.12 at the scattering angle of 140°-150° (Figure 4), we divided the regression into two parts: the regression with the scattering angle $< 115°$, and the one with scattering angle $\geq 115°$. Thus, the final parameterization of the VISvsSWIR surface BRF is:

$$\begin{aligned} R_{0.644/2.12} &= \frac{R_{dd,0.644}}{R_{dd,2.12}} \\ &= 0.00027\Theta + 0.5651 \end{aligned} \tag{4}$$

$$\begin{aligned} R_{0.466/2.12} &= \frac{R_{dd,0.466}}{R_{dd,2.12}} \\ &= \begin{cases} 0.00227\Theta + 0.00305; & (\Theta < 115°) \\ 0.00160\Theta + 0.08029; & (\Theta \geq 115°) \end{cases} \end{aligned} \tag{5}$$

By averaging over all the scattering angles, the ratios for 0.466vs2.12 and 0.644vs2.12 are about 0.25 and 0.58, respectively, which are quite similar to the ratios of 0.25 and 0.5 in Kaufman et al. (1997). Since the ratio is derived from the predefined dark surface, it is expected to be accurate over a vegetated area, and less accurate over a black soil and dry/dead vegetation area.

3 Results & Discussion

The BRF_DT2 algorithm was applied to the areas with different aerosol loading levels. Three cases were selected, where we have 2008 and 2010 two years of data from Eastern China (20°N - 50°N, 100°E - 125°E) and North America (25°N - 65°N, 135°W - 60°W), and four months (January and July in 2008 and 2010, respectively) of data from the global land areas, see

Atmos. Meas. Tech. Discuss., doi:10.5194/amt-2016-185, 2016
Manuscript under review for journal Atmos. Meas. Tech.
Published: 12 July 2016

Atmospheric Measurement Techniques Discussions

Table 1. Eastern China area gives the heaviest aerosol loading (AOD=0.39), whereas the global land and North America area give less, with the AOD of 0.15 and 0.1, respectively.

To better understand the difference among the DT algorithms, the MODIS C6_DT and BRF_DT AOD retrievals were also investigated in this study. The comparisons were divided into two parts: one is a cross-comparison of AOD retrievals among DT algorithms, the other is their performance through validation with AERONET AOD.

3.1 Cross Comparison among DT AODs

Figure 6 shows an example on 16 January 2008 over Argentina, which demonstrates the new AOD and the difference as compared between C6_DT and BRF_DT AOD. The AOD with the best quality QA=3 is presented, labeled as "QA3" in the figure. From the western coast to northwestern region, there are several surface types, including dense dark vegetation (farmland and forest), dry grass or bare soil, and green grass, respectively.

For the south of the image (light area to the left) in Figure 6 D, the difference of the AOD retrievals between BRF_DT2 and C6_DT is close to zero, although the $NDVI_{SWIR}$ varies greatly along the latitude direction over the same area (Figure 6 H). The omission of $NDVI_{SWIR}$ in the parameterization does not significantly affect the retrieval. Similar findings are also shown in north area of 35°S in the Figure.

In the "yellow ellipse" area shown in Figure 6, we can see that the AOD retrievals of BRF_DT and BRF_DT2 are spatially smoother than C6_DT. This to some degree demonstrates that the AOD retrievals in BRF_DT and BRF_DT2 are much less affected by the underlying surface. In other words, the anisotropic reflection of the surface is well characterized and estimated by these two algorithms.

For the whole land area shown in Figure 6, the difference of BRF_DT2 - BRF_DT AOD presents a strong dependence on the scattering angle, where a positive difference (0.08) was found at a small scattering angle ($\Theta \leq 130°$), and a negative difference (-0.08) at a large scattering angle ($\Theta \geq 150°$), while less dependence was found for the difference of BRF_DT2 - C6_DT AOD. We will further check the AOD difference between the algorithms in the validation section.

In Figures 7, 8 and 9, three histogram statistics of MODIS AOD (QA=3) were made for Eastern China and North America with four months (January, April, July and October in 2008) of data, and for the global land with two months (January and July in 2008) of data, respectively. Several AOD bins are presented ranging from -0.05 to 3.0, where each bin is labeled as one number (e.g., one bin labeled as -0.05 means the AOD between -0.05 and -0.03). Due to the mask of cloudy or cloud-contaminated pixels in ancillary data (8-day MCD043A1), the number of BRF_DT and BRF_DT2 retrievals was reduced by near one-seventh than C6_DT. Thus, the normalized frequency is given for each bin.

From the histograms, we can roughly see how the anisotropic reflection of the surface affects the AOD retrieval. With heavy aerosol loading (AOD > 0.2), the discrepancy of the AOD retrievals takes place between BRF_DT/BRF_DT2 and C6_DT. With heavy aerosol loading, the beam light is largely scattered by the atmosphere, where it presents much more diffuse radiation, while much less directional radiation presented. Thus, the reflectance at the TOA is mostly contributed by the atmosphere scattering and surface diffuse-related reflection (e.g., hemispherical-hemispherical and hemispherical-directional reflection). And this would make the AOD retrieval much less sensitive to the parameterization of surface BRF R_{dd}.

Atmos. Meas. Tech. Discuss., doi:10.5194/amt-2016-185, 2016
Manuscript under review for journal Atmos. Meas. Tech.
Published: 12 July 2016

With low aerosol loading (AOD < 0.2), a significant difference of the frequency was found from C6_DT/BRF_DT to the new algorithm. And it seems that the difference is dependent on the months or seasons. We can see that a relatively small difference presents in April and July over Eastern China and North America in Figure 7 and 8. The variation of vegetation amount as season or month changes is a key factor for the retrievals. For the Northern Hemisphere such as Eastern China and North America area, the vegetations are abundant in Spring (e.g., April) and summer (July) and less abundant in Autumn (October) and Winter (January). As a result, BRF_DT and BRF_DT2 give similar AOD retrievals for a vegetated area, and different retrievals for less vegetation land (e.g., sparse vegetation and bare soil). The different performance is caused by the difference of the surface BRF parameterization between these two algorithms.

In a more general and wide area — the global land area, the differences of the frequency are not so significant as that for Eastern China and North America. The differences are smaller in January, and larger in July compared to that for Eastern China and North America. This is because that for the global land the total vegetation amount does not vary too much over time.

Particularly, the negative retrievals (-0.05 $<$ AOD $<$ 0.0, the summary of the first three bins) are significantly reduced in the new algorithm, compared to that in C6_DT and BRF_DT. The reduction of the negative retrievals is more significant in North America area, with the decrease by 21% (-0.21 = 0.14-0.35) in January, and 8% in October. The reduction becomes small with only 5% for the global land area, and even smaller ($< 4\%$) for Eastern China area. Obviously, the negative retrievals tend to more likely appear for low aerosol loading area (e.g., North America) due to the algorithm uncertainty. To further clarify the reduction of the negative retrievals, we made similar histograms for light aerosol loading area: Brazil and Australia, shown in Figure 10. The corresponding geo-information for these areas is given in Table 2. We found that the reduction can be 6% - 15% and 12% - 28% for Brazil and Australia area in the new algorithm, respectively.

3.2 Validation with AERONET AOD

Petrenko et al. (2012) introduced a new method to validate satellite AOD with AERONET measurements. Following this method, we averaged MODIS AOD retrieval and AERONET measurement spatially and temporally. For each AERONET site, a circle of 25 km radius centered at the site was selected. Then the MODIS pixels in this circle were averaged. The possible pixels number is up to 25 in the circle. AERONET measurements during the ± 30 minutes interval centering on the Aqua satellite overpass time, were chosen and averaged. The AOD with the best quality (QA=3) is used here. For a valid collocation, at least 3 MODIS pixels and 2 AERONET measurements are required, following the rule in Levy et al. (2013). By this method, we evaluated the AOD accuracy of the DT algorithm against AERONET measurements, as well as the angular dependence of retrievals.

3.2.1 Overall Performance of the AOD retrieval

Results are compared with the C6_DT expected error/accuracy (EE) $\pm(0.05 + 15\%)$ over land. The statistics of the AOD retrieval give a small difference between BRF_DT and BRF_DT2, such as in Eastern China and North America, around 1% increase of the retrievals falling within EE was achieved in the new algorithm compared to BRF_DT, whereas for the global land area, the increase by 2.5% was found (see Figure 11), and 5% increase is given as compared to C6_DT.

Atmos. Meas. Tech. Discuss., doi:10.5194/amt-2016-185, 2016
Manuscript under review for journal Atmos. Meas. Tech.
Published: 12 July 2016

Atmospheric Measurement Techniques Discussions

The changes of the parameterization mainly have large effects on the AOD retrieval under light aerosol loading (AOD<0.2) (also discussed above). Although by comparing the percentage of retrievals falling within the EE, the increase in North America is not significant between BRF_DT and BRF_DT2 AOD, it does not really mean a small changes between them since the current expected accuracy level $\pm$(0.05+15%) gives too much tolerance for the low aerosol loading area (North America). If we narrow the expected accuracy level like $\pm$(0.03+10%), and apply it to north America area, the difference becomes 5.5% (BRF_DT2 - BRF_DT: 64.96%-59.49%). Nevertheless, this accuracy level is so strict that the new retrievals can not meet the requirement of 1-σ interval (66%).

3.2.2 Angular Performance of the AOD retrieval

In order to test whether the AOD retrieval is dependent on the scattering angle, the MODIS AOD collocated with AERONET measurements were sorted and grouped into several equal bins by the scattering angle, where 8 bins were for Eastern China and 20 bins for North America and the global land area.

Figure 12 presents the AOD errors of DT algorithms as a function of scattering angle, where the errors are defined as the absolute difference of MODIS - AERONET AOD at 0.55 μm. The AOD retrievals filtered by QA3 were used here. Several statistics are reported for each bin. The statistics are the 1-σ interval and median ("star or circle") of AOD errors.

Generally, the errors of the AOD retrievals in all the algorithms vary with the scattering angle. We can see that the 1-σ errors increase with the increase of the scattering angle. This is mainly due to the estimation accuracy of the surface contribution varying with the scattering angle. The AOD retrieval is expected to be accurate in the DT algorithms when a dark surface is observed, since the TOA reflectance is mainly contributed by the atmosphere and little by the surface. Normally, the surface appears darker in the forward scattering angle (eg., $\Theta < 115°$, many shadows observed) while it appears brighter in the backscattering angle (few shadows observed).

The new algorithm presents apparent advantages in the AOD retrieval compared to C6_DT, where the errors of the 1-σ and median, are getting smaller, especially for Eastern China area. This is mainly due to the accurate estimation of the surface anisotropic reflection in the new algorithm.

The 1-σ errors in the three cases are quite similar between BRF_DT and the new algorithm. Due to angular effect of $NDVI_{SWIR}$ in the C6 parameterization, it leads to a less constraint on the spectral surface reflectance, resulting in less accurate retrievals than we expected. Conversely, this proves again the conclusion that the removal of $NDVI_{SWIR}$ in the new parameterization would not give a large error in the AOD retrieval.

It is interesting that the median errors are different between these two algorithms. Over the global land area, the angular bias is largely corrected in the new algorithm compared with BRF_DT, where at small and large scattering angles ($\Theta < 130°$ and $\Theta > 150°$) the errors of around -0.025 (-15%) and 0.04 (20%), are reduced to $\pm$0.01 ($\pm$5%). The angular correction was also found over North America, although there is still a little positive bias in the new algorithm, over all the scattering angles. As for Eastern China area, it shows the quite small correction where the median errors are mostly the same between BRF_DT and the new algorithm. This illustrates that by applying the new parameterization the angular effects of AOD retrieval can be

Atmos. Meas. Tech. Discuss., doi:10.5194/amt-2016-185, 2016
Manuscript under review for journal Atmos. Meas. Tech.
Published: 12 July 2016

Atmospheric Measurement Techniques Discussions

corrected over light aerosol loading area (e.g, North America with AOD < 0.2), while it would not be corrected over heavy aerosol loading area (e.g, Eastern China with AOD > 0.2).

Atmos. Meas. Tech. Discuss., doi:10.5194/amt-2016-185, 2016
Manuscript under review for journal Atmos. Meas. Tech.
Published: 12 July 2016

Atmospheric Measurement Techniques Discussions

4 Conclusions

In the AOD retrieval with satellite measurements, the accurate estimation of the surface contribution is a key process. Benefiting from the accurate estimation of the surface anisotropic reflectance, the BRF_DT algorithm can yield a better retrieval as compared to C6_DT. However, applied in BRF_DT, the surface reflectance relationship inherited from MODIS C6_DT can lead to an angular dependence of the AOD retrieval. The problem is due to at least two possible issues. The relationship that is derived by assuming a lambertian surface, is not well suitable for the land surface BRF. The vegetation index $NDVI_{SWIR}$ applied in the relationship may have a directional effect, and needs to be reconsidered for the AOD retrieval.

To investigate and improve this situation, BRF_DT is further developed by using a new relationship for surface BRF (called BRF_DT2). 3 years of ASRVN BRF data was collected and filtered to select dark surface observations, to derive the new relationship. In this relationship, the surface BRF at both visible band 0.466- and 0.644 μm is given as a linear function of that at 2.12 μm and the scattering angle. To test the performance of the new algorithm, three areas with different aerosol loading were used: data from Eastern China (heavy aerosol loading, AOD=0.39), North America (light, AOD=0.1) and the global land area (medium, AOD=0.15). For the case studies, a cross-comparison among C6_DT, BRF_DT and BRF_DT2 AOD was discussed, as well as the validation with AERONET AOD. The results show that under light aerosol loading (AOD < 0.2) some improvements for the AOD retrieval can be achieved with the new algorithm compared to C6_DT and BRF_DT:

- The negative retrievals (-0.05 $< \tau_{0.55} <$ 0.0) were significantly reduced, where the reduction can be up to 20% - 28% for some occurrence of region especially for clean area (AOD < 0.15). The problem of a large number of negative AOD in C6_DT (Levy et al., 2013), and as well as in BRF_DT, was alleviated in the new algorithm.

- The percentage of the retrievals falling within the accuracy level EE=$\pm$(0.05+15%) increases 2.5% and 5% for the AOD retrieval over the global land area compared to BRF_DT and C6_DT, respectively. Although a small increase was found in light aerosol loading area North America as compared to BRF_DT, it can still give a significant increase (5.5%) with a stricter accuracy level $\pm$(0.03+10%).

- The angular bias of the AOD retrieval is largely corrected. At small and large scattering angles ($\Theta < 130°$ and $\Theta > 150°$), the underestimation (-15%) and overestimation (20%) of the retrieval in BRF_DT are reduced to $\pm$5% in the new algorithm, for the global land area. Similar findings are shown in North America, although a little positive bias of the retrieval remains.

Lacking the effective vegetation index, the uncertainty of the AOD retrieval was not substantially reduced in the new algorithm. The more effective index for vegetation amount or surface type needs to be developed for the AOD retrieval algorithm, such that a seasonal-dependent NDVI is applied in the second generation of Deep Blue AOD algorithm (Hsu et al., 2013) and yields a better result than the older Deep Blue (Hsu et al., 2013; Sayer et al., 2013).

Atmos. Meas. Tech. Discuss., doi:10.5194/amt-2016-185, 2016
Manuscript under review for journal Atmos. Meas. Tech.
Published: 12 July 2016

Atmospheric Measurement Techniques Discussions

Acknowledgements. We appreciate MODIS Team for freely-distributed MOD04 L2, MCD43A1 and ASRVN (Terra) data downloaded from LAADS (https://ladsweb.nascom.nasa.gov/data/search.html), and many principal investigators and managers for establishing and maintaining AERONET data. This work was partially supported by China Scholarship Council (CSC) under the Grant CSC No.201206040045.

Table 1. Information of three case studies. Here, the AOD for the cases is obtained by averaging the corresponding AERONET measurements.

Area	Lat	Long	Aerosol Loading	Period
Eastern China	20°N - 50°N	100°E - 125°E	Heavy (AOD=0.39)	2008 and 2010
North America	25°N - 65°N	135°W - 60°W	Light (AOD=0.1)	2008 and 2010
Global land	—	—	Medium (AOD=0.15)	Jan and Jul in 2008 and 2010

Table 2. The geoinformation of Brazil and Australia.

Area	Lat	Long
Australia	15°S - 35°N	105°E - 155°E
Brazil	20°S - 0°	55°W - 30°W

Atmos. Meas. Tech. Discuss., doi:10.5194/amt-2016-185, 2016
Manuscript under review for journal Atmos. Meas. Tech.
Published: 12 July 2016

Atmospheric Measurement Techniques Discussions

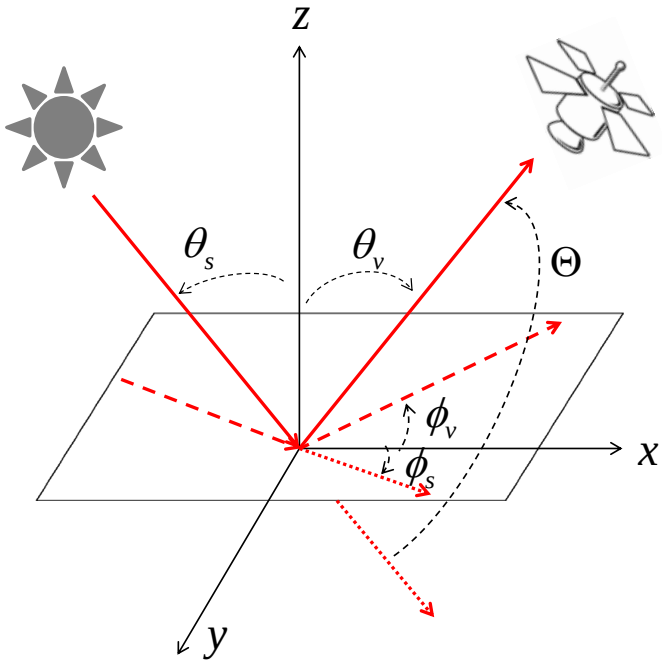

Figure 1. Schematic of illumination and viewing geometry on the surface target. The red solid lines (black dash curves) indicate the directions of the incident and reflected radiation, which are described as solar zenith angle θ_s and viewing zenith angle θ_v (measured from zenith direction z), and solar azimuth angle ϕ_s and viewing azimuth angle ϕ_v (measured from horizontal direction x). The dotted red lines represent the extension of the direction of the incident radiation. The scattering angle Θ is given as the angle between the direction of the incident radiation and the one of the reflected radiation recevied by the sensor.

Atmos. Meas. Tech. Discuss., doi:10.5194/amt-2016-185, 2016
Manuscript under review for journal Atmos. Meas. Tech.
Published: 12 July 2016

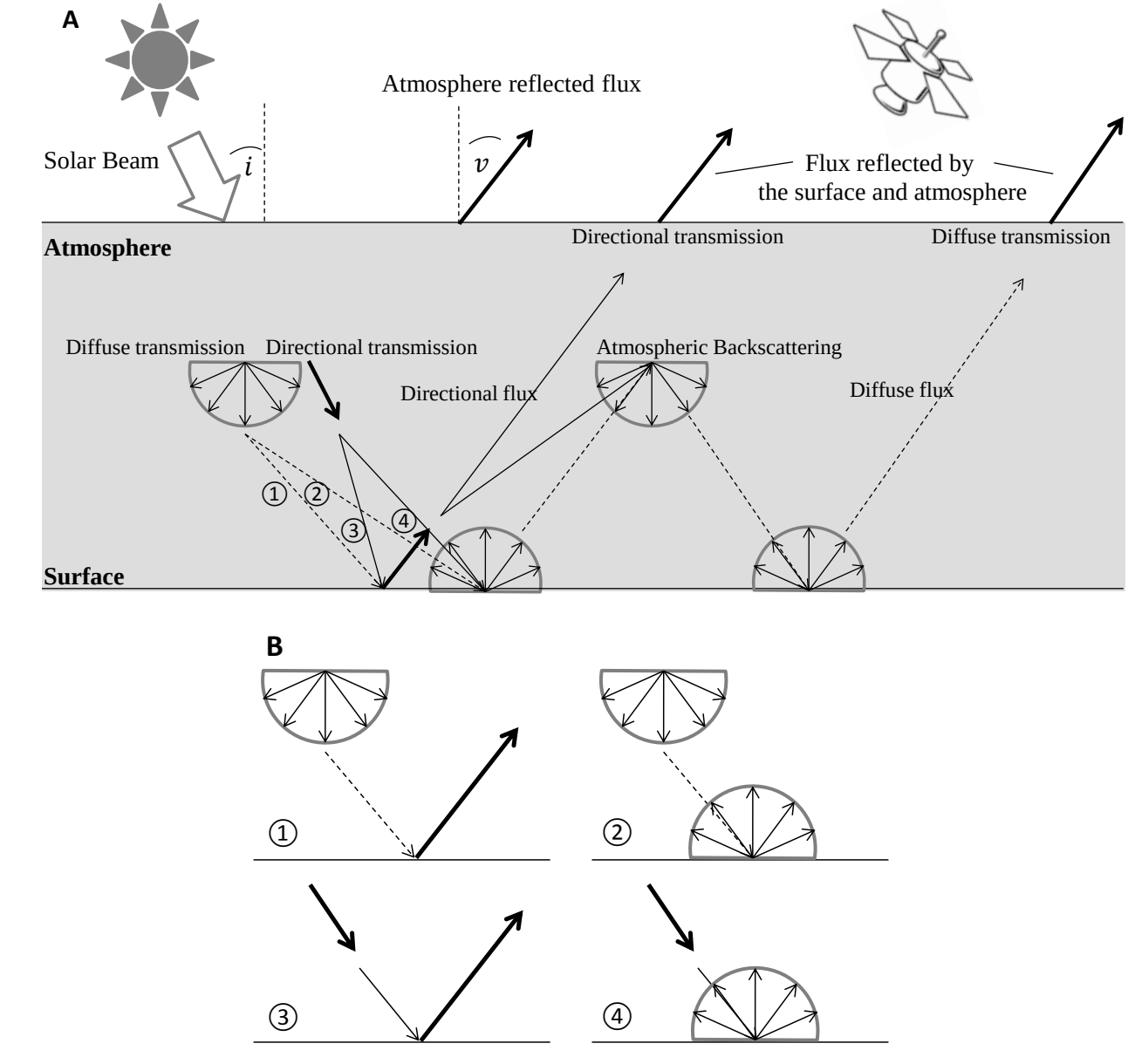

Figure 2. The TOA flux observed by the satellite considering the surface BRDF effects. The surface BRDF is simply described as 4 elements: hemispherical-directional ①, hemispherical-hemispherical ②, directional-directional ③ and directional-hemispherical reflectance/reflection ④, also shown in Figure B. More details are explained in the text.

Atmos. Meas. Tech. Discuss., doi:10.5194/amt-2016-185, 2016
Manuscript under review for journal Atmos. Meas. Tech.
Published: 12 July 2016

Atmospheric Measurement Techniques Discussions

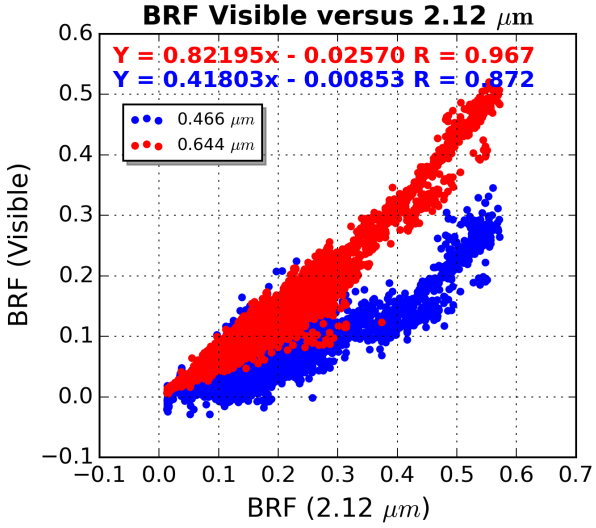

Figure 3. The surface BRF in visible wavelength (0.466- and 0.644 μm) compared with that in 2.12 μm wavelength, under AOD < 0.2.

Atmos. Meas. Tech. Discuss., doi:10.5194/amt-2016-185, 2016
Manuscript under review for journal Atmos. Meas. Tech.
Published: 12 July 2016

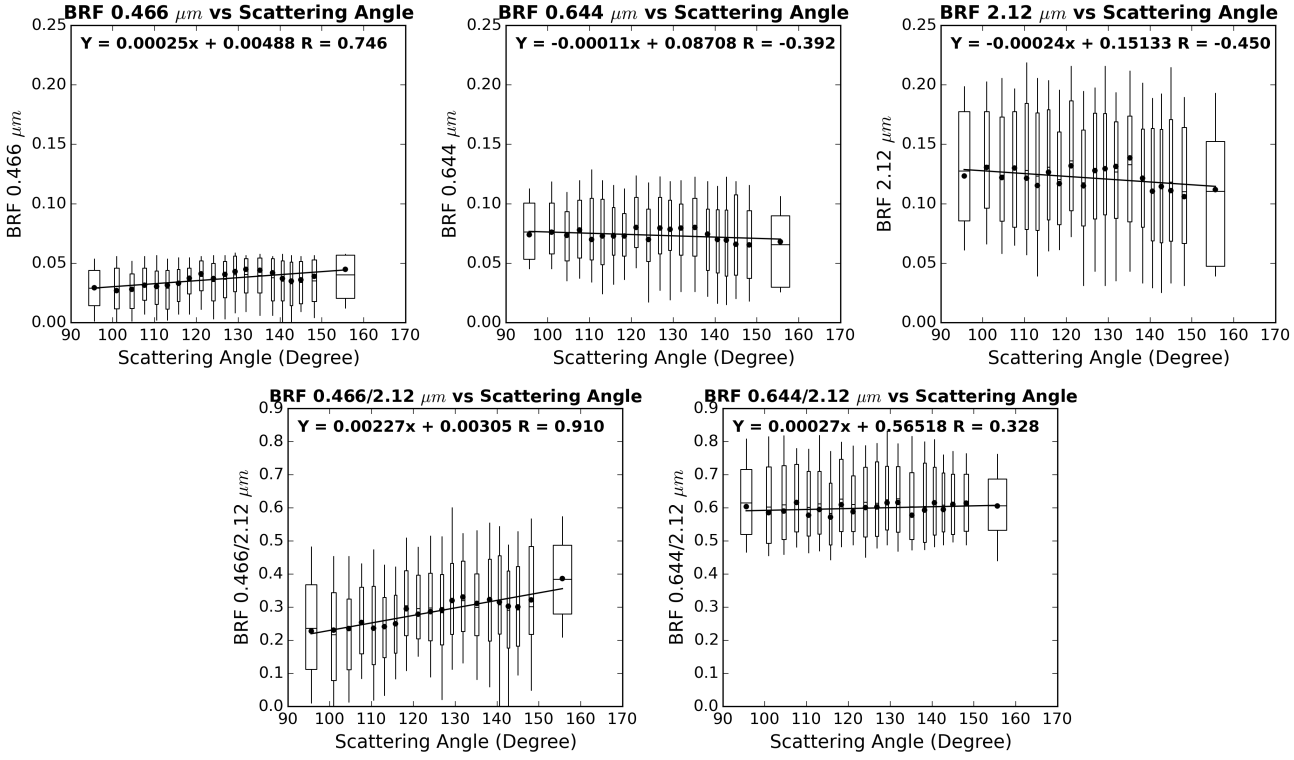

Figure 4. The VISvsSWIR surface BRF as a function of the scattering angle. The dataset (2739 cases) with the dark surface are sorted and grouped into 20 bins by the scattering angle. Each bin has around 140 cases. On all subplots, dot, the height of box and the length of whisker for each bin indicate the median value, 1-σ and 2-σ of the reflectance or ratios, respectively. And the width of box means 1-σ of the scattering angle for each bin. The first row shows the surface BRF at each wavelength (0.466-, 0.644- and 2.12 μm) as function of the scattering angle. And the second row shows the ratios of the surface BRF 0.466/2.12 and 0.644/2.12 as a function of the scattering angle.

Atmos. Meas. Tech. Discuss., doi:10.5194/amt-2016-185, 2016
Manuscript under review for journal Atmos. Meas. Tech.
Published: 12 July 2016

Atmospheric Measurement Techniques Discussions

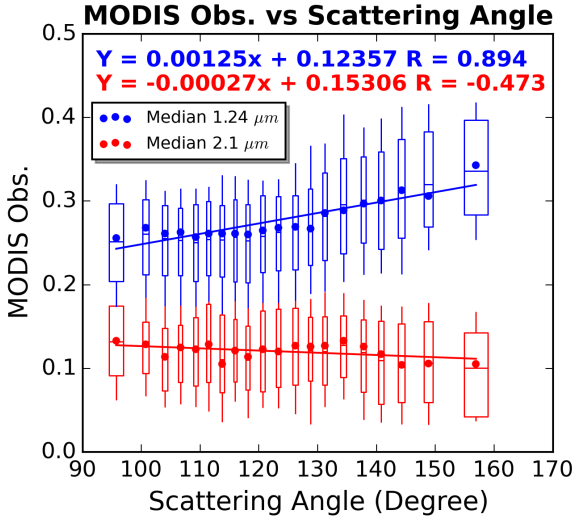

Figure 5. MODIS observation (Obs.) as a function of the scattering angle at 1.24- and 2.12 μm. "Blue" and "red" indicate the observation at 1.24- and 2.12 μm, respectively. Except for the color, other symbols are similar to Figure 4.

Atmos. Meas. Tech. Discuss., doi:10.5194/amt-2016-185, 2016
Manuscript under review for journal Atmos. Meas. Tech.
Published: 12 July 2016

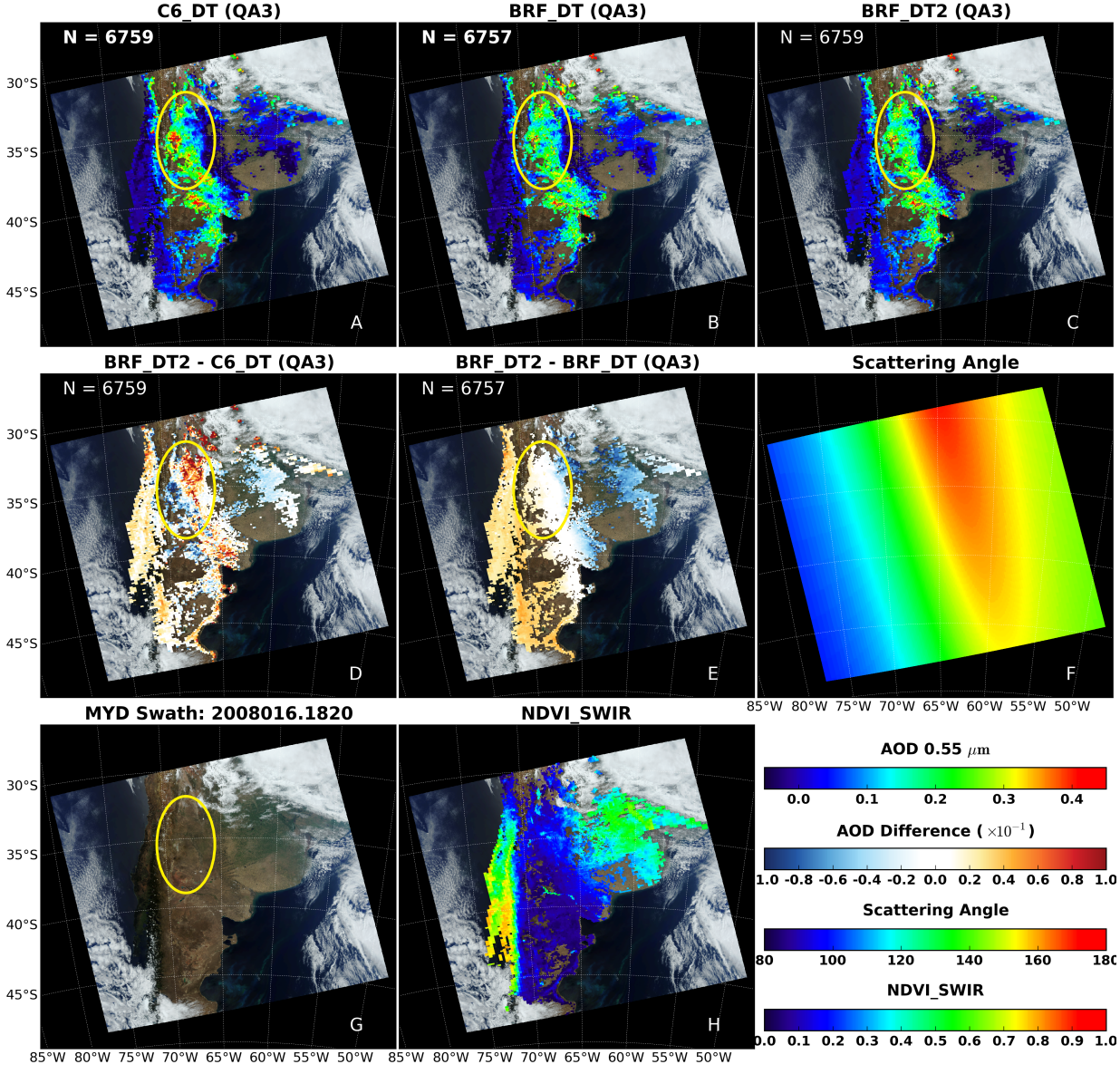

Figure 6. AOD over Argentina. Figure A-C show the AOD retrieved by the C6_DT, BRF_DT and BRF_DT2 algorithm. AOD with QA=3 was labeled as "QA3". Figure D and E show the AOD difference between DT algorithms. Figure F - H show the MODIS scattering anle, the MODIS RGB "true color" and $NDVI_{SWIR}$. The MODIS RGB image is obtained through combination of MODIS three channels 1, 4 and 3.

Atmos. Meas. Tech. Discuss., doi:10.5194/amt-2016-185, 2016
Manuscript under review for journal Atmos. Meas. Tech.
Published: 12 July 2016

Atmospheric Measurement Techniques Discussions

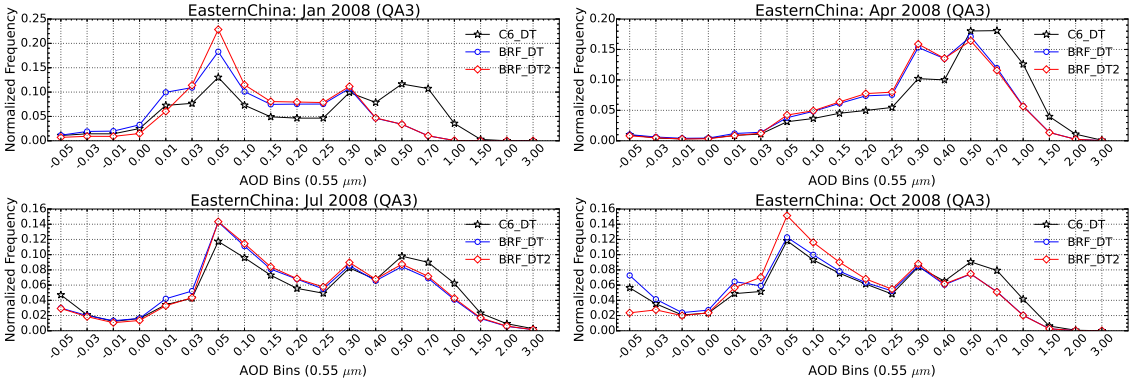

Figure 7. Histograms for Eastern China DT AOD (at 0.55 μm) from Aqua for four months. Plotted are data from C6_DT, BRF_DT and BRF_DT2 with QA=3, labeled as "QA3". Bin labels represent the lower boundary of the bin. For example, a bin labeled as -0.05 means the AOD between -0.05 and -0.03.

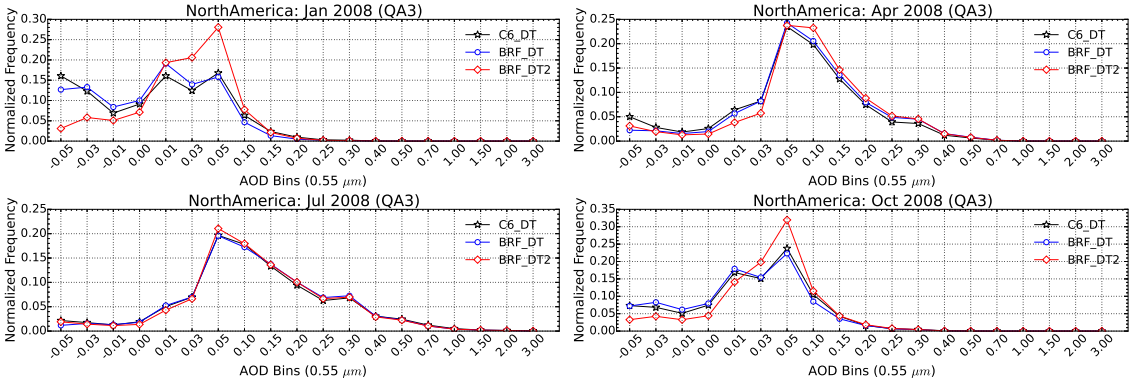

Figure 8. Histograms for North America DT AOD (at 0.55 μm) from Aqua for four months. Other symbols are similar to Figure 7.

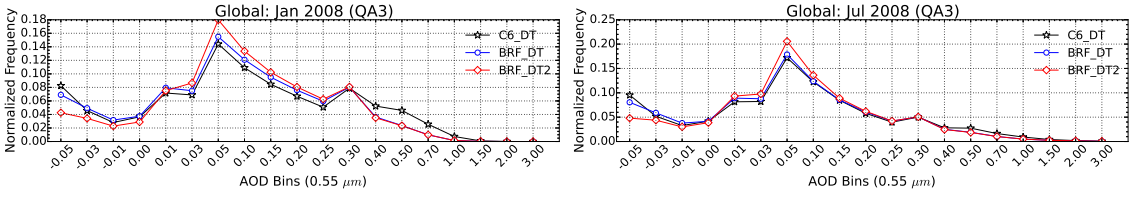

Figure 9. Histograms for the global land DT AOD (at 0.55 μm) from Aqua for two months. Other symbols are similar to Figure 7.

Atmos. Meas. Tech. Discuss., doi:10.5194/amt-2016-185, 2016
Manuscript under review for journal Atmos. Meas. Tech.
Published: 12 July 2016

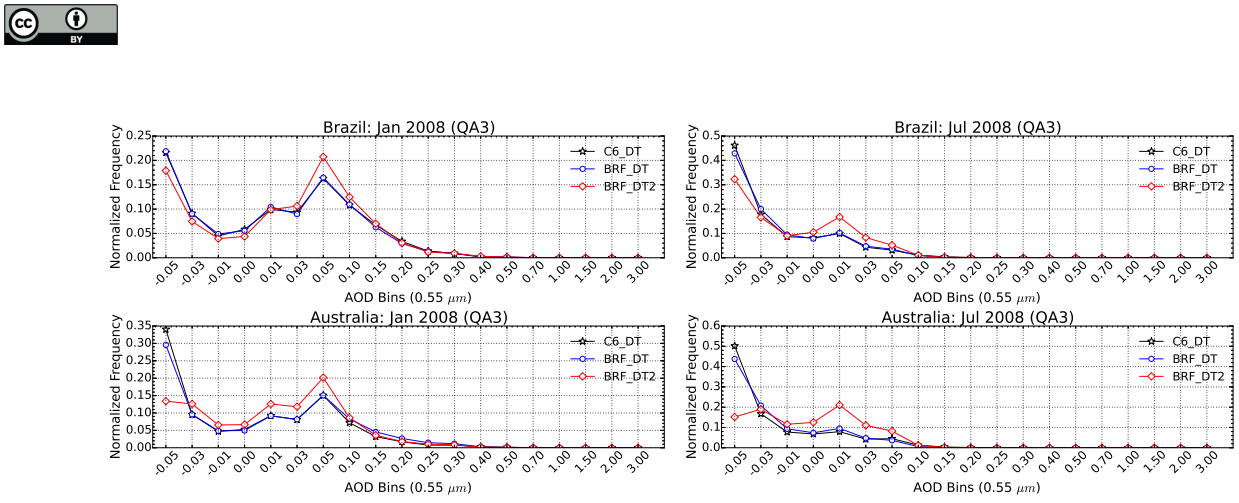

Figure 10. Histograms for the AOD (at 0.55 μm) in Brazil and Australia. The AOD data is from the global land area. Other symbols are similar to Figure 7.

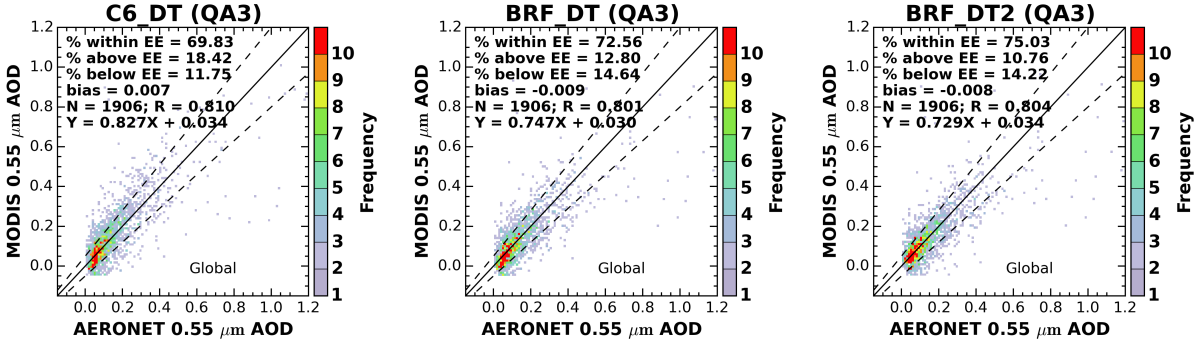

Figure 11. The comparison of AOD among the DT algorithms over the the global land. The DT algorithms are C6_DT, BRF_DT and BRF_DT2. The retrieved AOD is filtered with QA = 3, shown against AERONET AOD. The dash line is Expected Error (EE) $\pm(0.05+15\%)$ and the solid line is one-one line, respectively. Note that QA=3 is labeled as "QA3".

Atmos. Meas. Tech. Discuss., doi:10.5194/amt-2016-185, 2016
Manuscript under review for journal Atmos. Meas. Tech.
Published: 12 July 2016

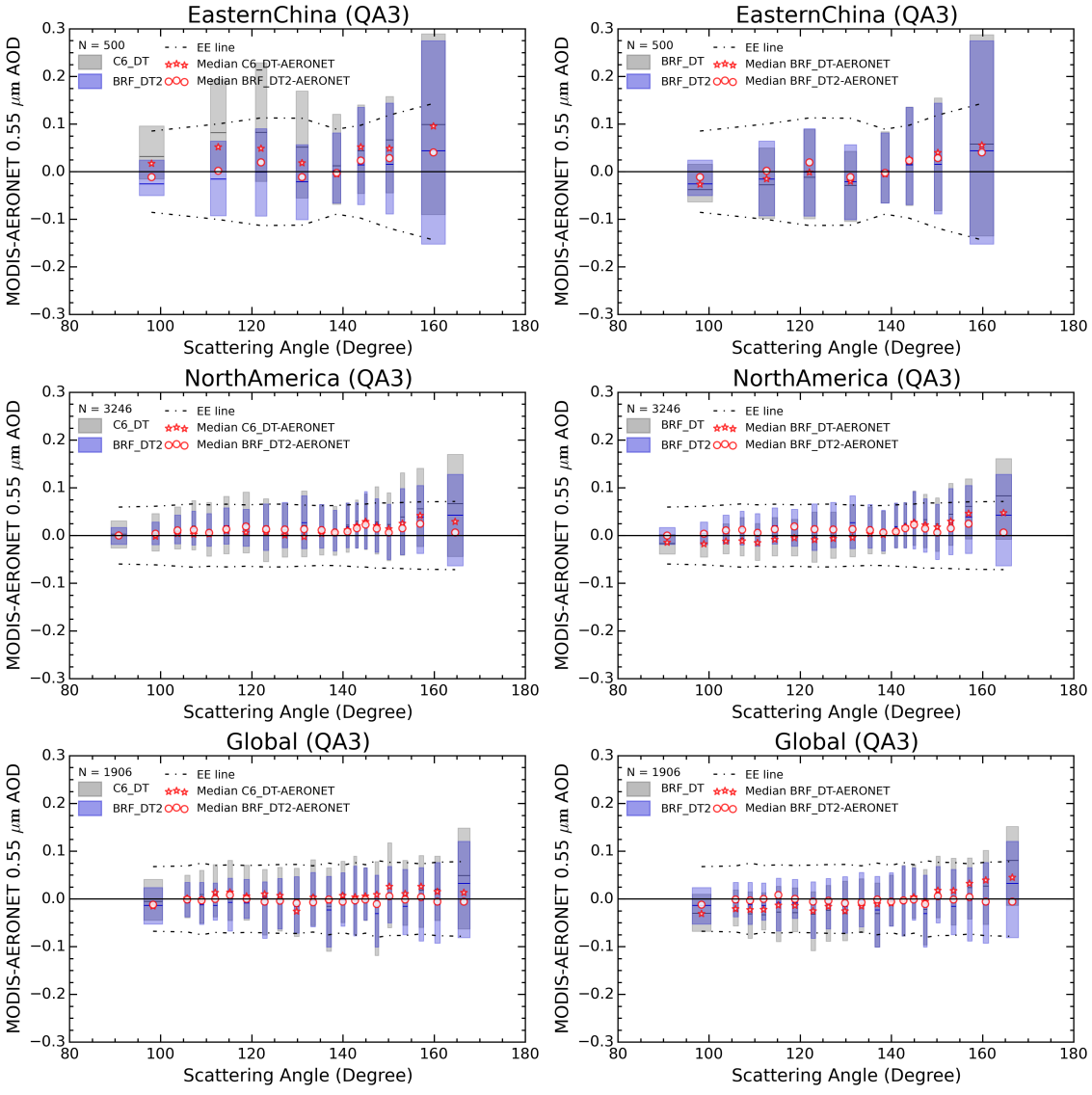

Figure 12. AOD at 0.55 μm error as a function of scattering angle with QA=3 (labeled as "QA3"). AOD error is defined as MODIS retrieved AOD - AERONET AOD, borken into euqal number bins of scattering angles, the data are plotted for Eastern China, North America and the global land respectively. The dash line and solid balck line is EE and zero error. For each box, width is 1-σ of the scattering angles bin, whereas height, middle line are the 1-σ, mean of the AOD error. Shown in the first and second column are the performace between C6_DT and BRF_DT2, and BRF_DT and BRF_DT2, respectively. The colored box "gray" is for C6_DT and BRF_DT, and "blue" ones are for BRF_DT2, whereas red symbols "star" are the median of AOD error for C6_DT and BRF_DT, and "circ" ones are for BRF_DT2.

Atmos. Meas. Tech. Discuss., doi:10.5194/amt-2016-185, 2016
Manuscript under review for journal Atmos. Meas. Tech.
Published: 12 July 2016

References

Chu, D. A., Kaufman, Y. J., Zibordi, G., Chern, J. D., Mao, J., Li, C., and Holben, B. N.: Global monitoring of air pollution over land from the Earth Observing System-Terra Moderate Resolution Imaging Spectroradiometer (MODIS), Journal of Geophysical Research: Atmospheres, 108, 4661, doi:10.1029/2002JD003179, http://onlinelibrary.wiley.com/doi/10.1029/2002JD003179/abstract, 2003.

Diner, D. J., Martonchik, J. V., Kahn, R. A., Pinty, B., Gobron, N., Nelson, D. L., and Holben, B. N.: Using angular and spectral shape similarity constraints to improve MISR aerosol and surface retrievals over land, Remote Sensing of Environment, 94, 155–171, doi:10.1016/j.rse.2004.09.009, http://www.sciencedirect.com/science/article/pii/S0034425704002937, 2005.

Dubovik, O., Herman, M., Holdak, A., Lapyonok, T., Taure, D., Deuze, J. L., Ducos, F., and Sinyuk, A.: Statistically Optimized Inversion Algorithm for Enhanced Retrieval of Aerosol Properties from Spectral Multi-Angle Polarimetric Satellite Observations, Atmospheric Measurement Techniques, 4, 975–1018, doi:10.5194/amt-4-975-2011, http://ntrs.nasa.gov/search.jsp?R=20120013673, 2011.

Engel-Cox, J. A., Holloman, C. H., Coutant, B. W., and Hoff, R. M.: Qualitative and quantitative evaluation of MODIS satellite sensor data for regional and urban scale air quality, Atmospheric Environment, 38, 2495–2509, doi:10.1016/j.atmosenv.2004.01.039, http://www.sciencedirect.com/science/article/pii/S1352231004001451, 2004.

Gatebe, C., King, M., Tsay, S.-C., Ji, Q., Arnold, G., and Li, J.: Sensitivity of off-nadir zenith angles to correlation between visible and near-infrared reflectance for use in remote sensing of aerosol over land, IEEE Transactions on Geoscience and Remote Sensing, 39, 805–819, doi:10.1109/36.917901, 2001.

Herman, J. R. and Celarier, E. A.: Earth surface reflectivity climatology at 340–380 nm from TOMS data, Journal of Geophysical Research: Atmospheres, 102, 28 003–28 011, doi:10.1029/97JD02074, http://onlinelibrary.wiley.com/doi/10.1029/97JD02074/abstract, 1997.

Hsu, N. C., Tsay, S.-C., King, M. D., and Herman, J. R.: Aerosol properties over bright-reflecting source regions, IEEE Transactions on Geoscience and Remote Sensing, 42, 557–569, doi:10.1109/TGRS.2004.824067, 2004.

Hsu, N. C., Tsay, S. C., King, M. D., and Herman, J. R.: Deep Blue Retrievals of Asian Aerosol Properties During ACE-Asia, IEEE Transactions on Geoscience and Remote Sensing, 44, 3180–3195, doi:10.1109/TGRS.2006.879540, 2006.

Hsu, N. C., Jeong, M.-J., Bettenhausen, C., Sayer, A. M., Hansell, R., Seftor, C. S., Huang, J., and Tsay, S.-C.: Enhanced Deep Blue aerosol retrieval algorithm: The second generation, Journal of Geophysical Research: Atmospheres, 118, 9296–9315, doi:10.1002/jgrd.50712, http://onlinelibrary.wiley.com/doi/10.1002/jgrd.50712/abstract, 2013.

IPCC: Working Group I Contribution to the IPCC Fifth Assessment Report (AR5)Climate Change 2013: The Physical Science Basis, Intergovernmental Panel on Climate Change, Geneva, Switzerland, 2013.

Kaufman, Y. J., Wald, A. E., Remer, L. A., Gao, B.-C., Li, R.-R., and Flynn, L.: The MODIS 2.1- mu;m channel-correlation with visible reflectance for use in remote sensing of aerosol, IEEE Transactions on Geoscience and Remote Sensing, 35, 1286–1298, doi:10.1109/36.628795, 1997.

Kaufman, Y. J., Tanré, D., and Boucher, O.: A satellite view of aerosols in the climate system, Nature, 419, 215–223, doi:10.1038/nature01091, http://www.nature.com/nature/journal/v419/n6903/abs/nature01091.html, 2002.

Koelemeijer, R. B. A., de Haan, J. F., and Stammes, P.: A database of spectral surface reflectivity in the range 335–772 nm derived from 5.5 years of GOME observations, Journal of Geophysical Research: Atmospheres, 108, 4070, doi:10.1029/2002JD002429, http://onlinelibrary.wiley.com/doi/10.1029/2002JD002429/abstract, 2003.

Laden, F., Neas, L. M., Dockery, D. W., and Schwartz, J.: Association of fine particulate matter from different sources with daily mortality in six U.S. cities., Environmental Health Perspectives, 108, 941–947, http://www.ncbi.nlm.nih.gov/pmc/articles/PMC1240126/, 2000.

Levy, R. C., Remer, L. A., and Dubovik, O.: Global aerosol optical properties and application to Moderate Resolution Imaging Spectroradiometer aerosol retrieval over land, Journal of Geophysical Research: Atmospheres, 112, D13 210, doi:10.1029/2006JD007815, http://onlinelibrary.wiley.com/doi/10.1029/2006JD007815/abstract, 2007a.

Levy, R. C., Remer, L. A., Mattoo, S., Vermote, E. F., and Kaufman, Y. J.: Second-generation operational algorithm: Retrieval of aerosol properties over land from inversion of Moderate Resolution Imaging Spectroradiometer spectral reflectance, Journal of Geophysical Research: Atmospheres, 112, D13 211, doi:10.1029/2006JD007811, http://onlinelibrary.wiley.com/doi/10.1029/2006JD007811/abstract, 2007b.

Levy, R. C., Mattoo, S., Munchak, L. A., Remer, L. A., Sayer, A. M., Patadia, F., and Hsu, N. C.: The Collection 6 MODIS aerosol products over land and ocean, Atmos. Meas. Tech., 6, 2989–3034, doi:10.5194/amt-6-2989-2013, http://www.atmos-meas-tech.net/6/2989/2013/, 2013.

Lucht, W., Schaaf, C., and Strahler, A.: An algorithm for the retrieval of albedo from space using semiempirical BRDF models, IEEE Transactions on Geoscience and Remote Sensing, 38, 977–998, doi:10.1109/36.841980, 2000.

Martonchik, J. V., Diner, D. J., Kahn, R. A., Ackerman, T. P., Verstraete, M. M., Pinty, B., and Gordon, H. R.: Techniques for the retrieval of aerosol properties over land and ocean using multiangle imaging, IEEE Transactions on Geoscience and Remote Sensing, 36, 1212–1227, doi:10.1109/36.701027, 1998.

McComiskey, A., Schwartz, S. E., Schmid, B., Guan, H., Lewis, E. R., Ricchiazzi, P., and Ogren, J. A.: Direct aerosol forcing: Calculation from observables and sensitivities to inputs, Journal of Geophysical Research: Atmospheres, 113, D09 202, doi:10.1029/2007JD009170, http://onlinelibrary.wiley.com/doi/10.1029/2007JD009170/abstract, 2008.

North, P. R. J.: Estimation of aerosol opacity and land surface bidirectional reflectance from ATSR-2 dual-angle imagery: Operational method and validation, Journal of Geophysical Research: Atmospheres, 107, AAC 4–1, doi:10.1029/2000JD000207, http://onlinelibrary.wiley.com/doi/10.1029/2000JD000207/abstract, 2002.

North, P. R. J., Briggs, S. A., Plummer, S. E., and Settle, J. J.: Retrieval of land surface bidirectional reflectance and aerosol opacity from ATSR-2 multiangle imagery, IEEE Transactions on Geoscience and Remote Sensing, 37, 526–537, doi:10.1109/36.739106, 1999.

Petrenko, M., Ichoku, C., and Leptoukh, G.: Multi-sensor Aerosol Products Sampling System (MAPSS), Atmos. Meas. Tech., 5, 913–926, doi:10.5194/amt-5-913-2012, http://www.atmos-meas-tech.net/5/913/2012/, 2012.

Pope III, C. A. and Dockery, D. W.: Health Effects of Fine Particulate Air Pollution: Lines that Connect, Journal of the Air & Waste Management Association, 56, 709–742, doi:10.1080/10473289.2006.10464485, http://dx.doi.org/10.1080/10473289.2006.10464485, 2006.

Pope III, C. A., Burnett, R. T., Thun, M. J., Calle, E. E., Krewski, D., Ito, K., and Thurston, G. D.: LUng cancer, cardiopulmonary mortality, and long-term exposure to fine particulate air pollution, JAMA, 287, 1132–1141, doi:10.1001/jama.287.9.1132, http://dx.doi.org/10.1001/jama.287.9.1132, 2002.

Remer, L., Wald, A., and Kaufman, Y.: Angular and seasonal variation of spectral surface reflectance ratios: implications for the remote sensing of aerosol over land, IEEE Transactions on Geoscience and Remote Sensing, 39, 275–283, doi:10.1109/36.905235, 2001.

Remer, L. A., Kaufman, Y. J., Tanré, D., Mattoo, S., Chu, D. A., Martins, J. V., Li, R.-R., Ichoku, C., Levy, R. C., Kleidman, R. G., Eck, T. F., Vermote, E., and Holben, B. N.: The MODIS Aerosol Algorithm, Products, and Validation, Journal of the Atmospheric Sciences, 62, 947–973, doi:10.1175/JAS3385.1, http://journals.ametsoc.org/doi/abs/10.1175/JAS3385.1, 2005.

Remer, L. A., Mattoo, S., Levy, R. C., and Munchak, L. A.: MODIS 3 km aerosol product: algorithm and global perspective, Atmos. Meas. Tech., 6, 1829–1844, doi:10.5194/amt-6-1829-2013, http://www.atmos-meas-tech.net/6/1829/2013/, 2013.

Rondeaux, G. and Vanderbilt, V. C.: Specularly modified vegetation indices to estimate photosynthetic activity, International Journal of Remote Sensing, 14, 1815–1823, doi:10.1080/01431169308954004, http://dx.doi.org/10.1080/01431169308954004, 1993.

Samet, J. M., Dominici, F., Curriero, F. C., Coursac, I., and Zeger, S. L.: Fine Particulate Air Pollution and Mortality in 20 U.S. Cities, 1987–1994, New England Journal of Medicine, 343, 1742–1749, doi:10.1056/NEJM200012143432401, http://dx.doi.org/10.1056/NEJM200012143432401, 2000.

Sayer, A. M., Hsu, N. C., Bettenhausen, C., and Jeong, M.-J.: Validation and uncertainty estimates for MODIS Collection 6 "Deep Blue" aerosol data, Journal of Geophysical Research: Atmospheres, 118, 7864–7872, doi:10.1002/jgrd.50600, http://onlinelibrary.wiley.com/doi/10.1002/jgrd.50600/abstract, 2013.

Schaaf, C. B., Gao, F., Strahler, A. H., Lucht, W., Li, X., Tsang, T., Strugnell, N. C., Zhang, X., Jin, Y., Muller, J.-P., Lewis, P., Barnsley, M., Hobson, P., Disney, M., Roberts, G., Dunderdale, M., Doll, C., d'Entremont, R. P., Hu, B., Liang, S., Privette, J. L., and Roy, D.: First operational BRDF, albedo nadir reflectance products from MODIS, Remote Sensing of Environment, 83, 135–148, doi:10.1016/S0034-4257(02)00091-3, http://www.sciencedirect.com/science/article/pii/S0034425702000913, 2002.

Verhoef, W.: Earth observation modeling based on layer scattering matrices, Remote Sensing of Environment, 17, 165–178, doi:10.1016/0034-4257(85)90072-0, http://www.sciencedirect.com/science/article/pii/0034425785900720, 1985.

Wang, Y., Lyapustin, A., Privette, J., Morisette, J., and Holben, B.: Atmospheric Correction at AERONET Locations: A New Science and Validation Data Set, IEEE Transactions on Geoscience and Remote Sensing, 47, 2450–2466, doi:10.1109/TGRS.2009.2016334, 2009.

Wu, Y., Guo, J., Zhang, X., Tian, X., Zhang, J., Wang, Y., Duan, J., and Li, X.: Synergy of satellite and ground based observations in estimation of particulate matter in eastern China, Science of The Total Environment, 433, 20–30, doi:10.1016/j.scitotenv.2012.06.033, http://www.sciencedirect.com/science/article/pii/S0048969712008595, 2012.

Wu, Y., de Graaf, M., and Menenti, M.: MODIS Aerosol Optical Depth retrieval over land considering surface BRDF effects, submitted to IEEE, 2016.